Journal of Molecular Catalysis A: Chemical 348 (2011) 55–62

Contents lists available at ScienceDirect

Journal of Molecular Catalysis A: Chemical

journal homepage: www.elsevier.com/locate/molcata

Direct catalytic decomposition of NO with Cu–ZSM-5: A DFT–ONIOM study

Rodolfo Izquierdo[a,*], Leonardo J. Rodríguez[a,1], Rafael Añez[b], Aníbal Sierraalta[b]

[a] Laboratorio de Química Teórica y Computacional (LQTC), Departamento de Química, Facultad Experimental de Ciencias, Universidad del Zulia, Apartado 526, Maracaibo, Venezuela
[b] Laboratorio de Química Computacional, Centro de Química, Instituto Venezolano de Investigaciones Científicas, Apartado 21827, Caracas 1020-A, Venezuela

ARTICLE INFO

Article history:
Received 17 January 2011
Received in revised form 27 July 2011
Accepted 29 July 2011
Available online 5 August 2011

Keywords:
ONIOM
DFT
NO decomposition
Copper mononitrosyl
Cu–ZSM-5

ABSTRACT

ONIOM calculations for the direct catalytic decomposition mechanism of NO_2 and NO by Cu–ZSM-5 were carried out. In two layer calculations, Density Functional Theory and Universal Force Field were employed for the high and low level models, respectively. ΔH° and ΔG° evaluations were performed in order to determine the thermodynamically more favored way for catalytic decomposition of NO_2 and NO. The results show that a novel copper κ^2 mononitrosyl species (Z–^{2}Cu–κ^2NO) is in equilibrium with the Z–^{2}CuNO and Z–^{2}CuON species. According to our results, the Z–^{2}Cu–κ^2NO species is the intermediary key of the direct catalytic decomposition mechanism of NO_2 and NO by Cu–ZSM-5.

1. Introduction

Although the NO_2 and NO (NO_x) play an important role as precursor of tropospheric ozone [1], they are extremely harmful contaminants to the environments [2,3]. The global NO_x emissions have increased approximately from 12 Tg N yr^{-1}, before the industrial development, to 40–50 Tg N yr^{-1} nowadays [4,5]. The high NO_x concentrations are responsible for photochemical smoke, green house effect, acid rain and many respiratory diseases in everywhere [6–8]. The NO_x decomposition to N_2 and O_2 (deNO_x) is a very important process in the environmental catalysis field. Despite their thermodynamic instability, the NO_x decomposition to N_2 and O_2 is kinetically unfavorable implying that efficient catalysts are necessary to eliminate the NO_x [9–11].

Porous materials have gained acceptance as catalysts for the industrial and environmental applications [12–17]. Among these, zeolites are one of the most studied catalysts for the deNO_x reaction [18–20]. On the other hand, when transition metals are embedded into a zeolite, they show higher catalytic activity and selectivity for deNO_x. For example, Co-exchanged zeolite [21,22], Pd-MOR [23–26] and Fe–ZSM-5 [21,27] showed high activity for the selective catalytic reduction (SCR) of NO_x. Specially, the Cu–ZSM-5 system has shown the highest catalytic activity for the direct catalytic decomposition of NO_x (DCD-NO_x) to produce N_2 and O_2 [28–30]. As reduction agent is not necessary, the DCD-NO_x process is an attractive way to remove the NO_x [31]. Despite the considerable experimental efforts have been made to understand the Cu–ZSM-5 catalytic behavior [30,32–38], the mechanism and active site nature still remain unclear [31]. Infrared (IR) studies at room temperature have shown the coexistence of the species: Z–Cu$^+$(NO), Z–Cu$^+$(NO)$_2$, Z–Cu^{2+}(NO), and Z–Cu^{2+}O$^-$(NO), as well as adsorbed N_2O, NO_2, N_2O_3, and NO_3^- [9,27,39,40] (where Z = ZSM-5). On the other hand, in situ IR studies have shown two bands corresponding to NO adsorbed on Z–Cu$^+$(NO) and Z–Cu^{2+}(NO) with stretching frequencies of 1814 cm^{-1} and 1905 cm^{-1}, respectively. Bands at 1825 and 1730 cm^{-1} have been assigned to symmetric and asymmetric normal modes of dinitrosyl species (Z–Cu$^+$(NO)$_2$) and bands at 1624 and 1565 cm^{-1}, to bridging and chelating coordination modes of Z–Cu^{2+}(NO_3^-) species [9,41–43].

Different reaction mechanisms for DCD-NO_x by Cu–ZSM-5 have been proposed in the literature. Some authors [9,39,40,44–47] have proposed that two NO molecules absorb on the active site (Z–Cu) to produce Z–CuO species and N_2O. The N_2O molecules can either react with Z–CuO to produce Z–CuO_2 and N_2 [39,40,44,45,47] or react with the active site and decompose in adsorbed O atoms and N_2 [46]. The adsorbed O atoms can react with NO_2 to produce NO_3, which decomposes in adsorbed O_2 and free NO. In general, the active sites are regenerated by O_2 desorption. On the other hand, different type of active sites have been proposed too, such as ZCuO [48], where the reaction mechanism takes place through a pathway that involve two NO molecules with ZCuO to produce Z–CuO_2 and N_2O through a ZCu(OONNO)-like transition state. Consequently, the latter discussion suggests that there is no agreement in the literature about the most probable way for the DCD-NO_x,

* Corresponding author. Tel.: +58 261 7597794; fax: +58 261 7597794.
E-mail address: reis131182@gmail.com (R. Izquierdo).
[1] In memory of Dr. Leonardo Rodríguez, professor, scientist and friend.

1381-1169/$ – see front matter © 2011 Elsevier B.V. All rights reserved.
doi:10.1016/j.molcata.2011.07.018

Table 1
Geometrical parameters, net charges and energy changes for the Cu^+ and Z–Cu systems.

System	Cu–O1 (Å)	Cu–O2 (Å)	O1–Cu–O2 (degree)	Q_{Cu} a.u.	$\Delta E_{LUMO-HOMO}$[a] (kcal mol^{-1})	ΔE[b] (kcal mol^{-1})
$^1Cu^+$	–	–	–	1.00	114.1	–
$^3Cu^+$	–	–	–	1.00	–	68.7
Z–^{1}Cu	1.989	2.040	74.8	0.94	86.5	–
Z–^{3}Cu	1.947	1.993	74.9	0.73	–	41.4

[a] Band gap.
[b] Energy changes for the transition between the singlet to triplet state.

mechanism, whereby more experimental and theoretical researches are necessary.

To explain the catalytic activity, several theoretical calculations have been devoted to analyze the NO decomposition over Cu–ZSM-5 [39,40,44,45,49–55]. Schneider and coworkers [45] simulated a single Si site (T-site) model of the ZSM-5 using the local spin density approximation (LSDA) and valence double-ζ plus polarization Slater-type basis set. These authors proposed an Eley–Rideal type process, where one NO is adsorbed in an activated O-down conformation Z–CuON to form the isonitrosyl intermediates (reaction (1)). Z–CuON reacts with a second NO to form a triplet state intermediate which produces N_2O (reaction (2)).

$$Z\text{–}Cu + NO \rightarrow Z\text{–}CuON \quad (1)$$

$$Z\text{–}CuON + NO \rightarrow Z\text{–}CuO + N_2O \quad (2)$$

However, Schneider and coworkers [45] were unable to identify a reaction pathway to produce Z–CuO and N_2O from the Z–Cu$(NO)_2$ or Z–CuNO. These results suggest that the Z–Cu$(NO)_2$ or Z–CuNO are not intermediates in the NO decomposition mechanism. On the other hand, Bell and coworkers [39,40] calculated the ΔG° and ΔH° values for many possible elementary reactions using Density Functional Theory (DFT) and statistical mechanics. Bell proposed a four reaction pathway:

$$Z\text{–}Cu + NO \rightarrow Z\text{–}CuNO \quad (3)$$

$$Z\text{–}CuNO + NO \rightarrow Z\text{–}CuO + N_2O \quad (4)$$

$$Z\text{–}CuO + N_2O \rightarrow Z\text{–}Cu\text{–}O_2 + N_2 \quad (5)$$

$$Z\text{–}CuO_2 \rightarrow Z\text{–}Cu + O_2 \quad (6)$$

Building a reliable system to model the zeolite active site could be a very hard work in terms of time and computational expense. A large number of atoms are necessary to represent correctly the zeolite cavity, thereby making difficult the use of quantum mechanism methodologies to study these systems. Recent development of hybrid methods such as embedded cluster or combined quantum mechanics/molecular mechanics (QM/MM) [56–58] has been used to study the adsorption properties and reaction mechanics of organic and inorganic molecules over different types of zeolite catalysts. In particular, the ONIOM (Our-own-N-layer Integrated molecular Orbital + molecular mechanics) method [59–61] has shown considerable promise for the study of zeolite using minimal computational requirements [17,62–65]. With this approach, large models can be used in order to investigate confinement effects and non-local interactions between the adsorbates and zeolite. The confinement effects are explicitly included and therefore, accurate results could be reached with less expensive models.

The present work was undertaken in order to help in the understanding of the chemistry associated with the NO_x decomposition over Cu–ZSM-5 catalyst. We analyze using ONIOM–DFT methods, three proposed mechanisms in the literature, by Schneider and coworkers [44,45,49], Chakraborty and coworkers [39,40] and Iglesia coworkers [46]. Thermodynamic and energetic aspects of the proposed mechanisms are analyzed to gain insight into the NO_x decomposition reactions over Cu–ZSM-5 catalyst.

2. Computational details

All calculations were carried out using the two layer ONIOM methodology [62–65] from the Gaussian-03 (G03) package [66]. The Universal Force Field (UFF) [67] for the low level and DFT (B3LYP) with the basis set 6-311++G(d,p) [68] for the high level calculations were employed. Calculated vibrational frequencies were scaled by a factor of 0.9679 [69]. The electronic charge distribution was analyzed using the natural bond orbital (NBO) scheme [70,71]. Thermodynamic property calculations (free energy (ΔG°) and enthalpy (ΔH°)) were performed at 850 K and 2 atm to simulate the experimental conditions [38,46,72].

In the ZSM-5 unit cell, there are 12 different T-sites. According to theoretical studies [27,73,74], the T12 site is the most favorable location for the substitution of Si by an Al atom. The negative charge created by the substitution is compensated by H^+ (Brønsted site) which can be exchanged by Cu^+. The high level model used in this work consists in five tetrahedrons (5T, see Fig. 1) which contain the T12 site. One Cu atom is placed on the T12 (Z–^{1}Cu, the superscript indicates the spin multiplicity) representing the exchanged Cu^+. The real model has 217 atoms, 10 atoms at high level and 207 atoms at low level (see Fig. 1). The cluster was saturated with H atoms to satisfy the edge atom valences and also, H atoms were used as link between the high and low level models. Similar models have been used in the literature to study the Cu–ZSM-5 catalyst [39,45,48–51].

3. Results and discussion

3.1. Characterization of Cu–ZSM-5 and NO–Cu–ZSM-5 systems

According to the literature [75–77], aggregates of Cu^+ atoms (pairs) are formed at low Si/Al ratios due to the interaction between to interchanged Cu^+ atoms. In this work, we are interested in catalysts with high Si/Al ratios and very dispersed Al atoms where no interaction between Cu^+ must be found. Thus, only the structure and behavior of monovalent atomically dispersed, single Cu ions in cationic sites will be discussed. Table 1 shows geometrical parameters, net charges and energy changes for the free Cu^+ atom and Z–Cu system in the singlet and triplet states. The Cu–O distances (see Fig. 1 and Table 1) in triplet state (Z–^{3}Cu) are shorter than that in singlet state (Z–^{1}Cu) and the net charge on Cu in Z–^{3}Cu (0.73e) is lower than that in Z–^{1}Cu (0.94e). The singlet → triplet transition energy (ΔE) is greater for gas phase Cu^+ than for Z–Cu. According to these results, it is clear that the zeolitic framework helps in the stabilization of excited states. The stabilization of the triplet state by the zeolitic framework is due to the fact that the transition electronic configuration d^9s^1 in the Cu reduces the repulsion between the electrons of the *d* orbital and the zeolitic O atoms.

It is well known that Z–Cu exhibits a strong N_2 adsorption at room temperature ($\Delta H^\circ = -17.9$ kcal mol^{-1}) [78]. According to Fourier transformed IR (FTIR) studies [42], the band at 2295 cm^{-1} corresponds to the stretching frequency (ν_{NN}) of N_2 adsorbed on Z–^{1}Cu. Table 2 shows ΔH°, geometries and vibrational frequencies for N_2 and H_2 molecules adsorbed on free Cu^+ atom and Z–^{1}Cu (see Fig. 2). For the $^1Cu^+$–N_2 system, the calculated ν_{NN} and N_2

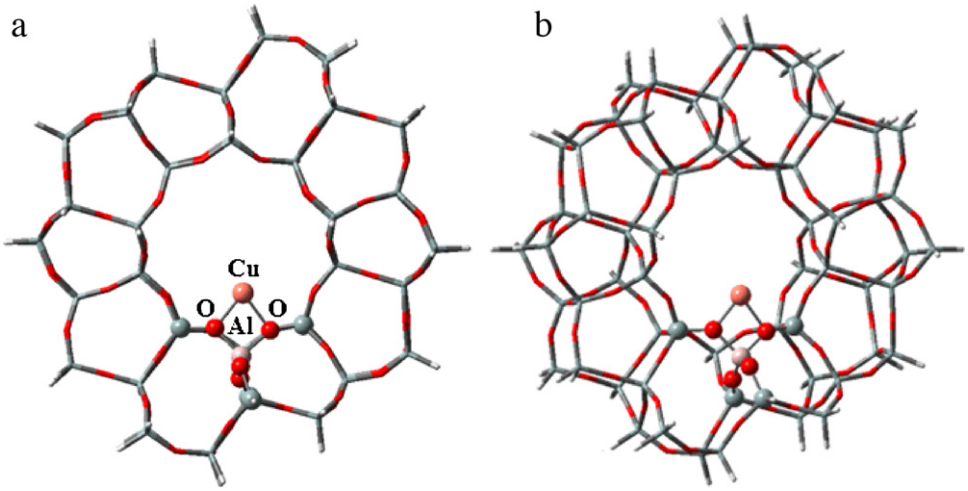

Fig. 1. Cu–ZSM-5 model (Z–Cu). Minimum energy structure (a) front view and (b) lateral view. High level, ball-stick. Low level, tube. O, red; Si, grey; Al, pink; Cu, orange. (For interpretation of the references to color in this figure legend, the reader is referred to the web version of the article.)

Table 2
ΔH°, geometrical parameters, net charges and vibrational frequencies for the adsorption of N_2 and H_2 on atomic $^1Cu^+$ and Z–^{1}Cu.

System	ΔH° (kcal mol^{-1})	Cu–X[a] (Å)	X–X[a] (Å)	Cu–X–X[a] (degree)	Q_{Cu} a.u.	ν_{XX} (cm^{-1})
$^1Cu^+$–N_2	−22.7	1.945	1.096	180.0	0.99	2366 ± 37
Z–^{1}Cu–N_2	−20.3	1.850	1.102	179.5	0.95	2298 ± 37
$^1Cu^+$–κ^2H_2	−16.7	1.750	0.787	77.0	0.97	3677 ± 37
Z–^{1}Cu–κ^2H_2	−19.3	1.623	0.815	75.5	0.90	3273 ± 37

[a] X = N or H. Free N_2: N–N = 1.095 Å; ν_{NN} = 2367 cm^{-1}; Free H_2: H–H = 0.744 Å; ν_{HH} = 4276 cm^{-1}.

bond distance are similar to the free N_2 which indicates a poor π-back donation from the Cu^+ *d* electrons to the N_2 antibonding π^* orbital. However, the ν_{NN} obtained in the Z–^{1}Cu–N_2 system is lower (69 cm^{-1}) than the corresponding values for free N_2. This suggests a considerable π-back donation from the Cu *d* electrons to the N_2 antibonding π^* orbitals. The N_2 stretching frequency (2298 cm^{-1}) and the ΔH° (−20.3 kcal mol^{-1}) values calculated herein are in good agreement with the experimental values reported by Datka and coworkers [42], and Kuroda [78]. Experimental studies have shown that Z–^{1}Cu exhibits a strong H_2 adsorption at room temperature with a band located at 3300 cm^{-1} (shift of 1000 cm^{-1} with respect to the free H_2), assigned to the H_2 stretching frequency (ν_{HH}) [79]. In order to test if our model is able to reproduce this shift, the adsorption of H_2 on the Z–^{1}Cu was performed. The results show that, on the Z–^{1}Cu the H_2 bond length increases with respect to free H_2. The theoretical ν_{HH} shift for Z–^{1}Cu–κ^2H_2 is 1003 cm^{-1} which is in good agreement with the experimental results of Kazansky and Pidko [79]. The H_2 frequency shift for the $^1Cu^+$–κ^2H_2 system is lower than the corresponding to the Z–^{1}Cu–κ^2H_2 system. This result shows clearly the electronic effects of the zeolitic framework on the adsorption properties and also, that the Z–^{1}Cu model and the methodology employed seem to be appropriate for modeling the Cu–ZSM-5 catalysts active site.

Table 3 shows some geometrical parameters, net charges, and calculated vibrational frequencies for the adsorption of one NO, two NO, NO_2 and NO_3 molecules on Z–^{1}Cu. The minimum energy

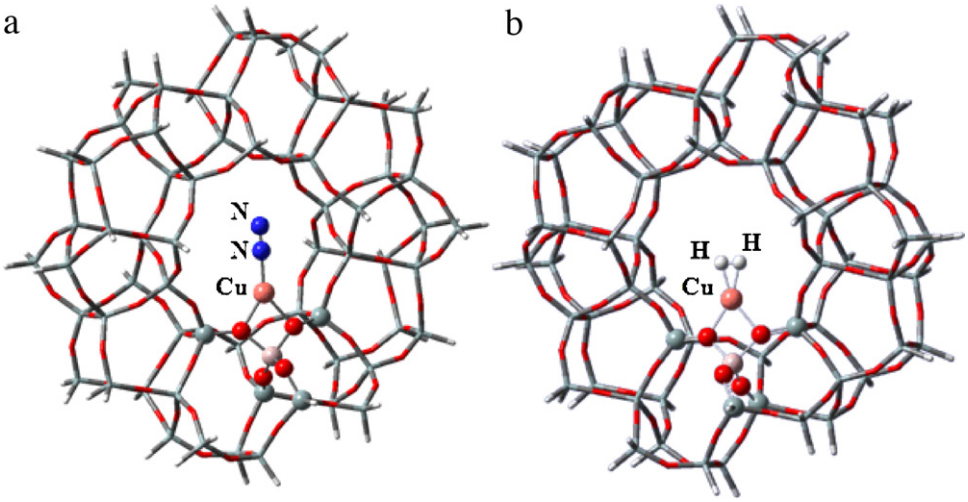

Fig. 2. Minimum energy structures: (a) κ^1–N_2 mode and (b) κ^2–H_2 mode. High level, ball-stick. Low level, tube. O, red; Si, grey; Al, pink; Cu, orange; N, blue and H, white. (For interpretation of the references to color in this figure legend, the reader is referred to the web version of the article.)

Table 3
Geometrical parameters, net charges and vibrational frequencies for NO, NO_2 and NO_3 adsorption on Z–^{1}Cu.

System	N–O (Å)	O–N–O (degree)	ν_{NO}[a] (cm^{-1})	ν_{NO2}[b] (cm^{-1})	ν_{NO2}[c] (cm^{-1})	ν_{NO3}[b] (cm^{-1})	ν_{NO3}[c] (cm^{-1})
NO	1.148	–	1916				
NO^-	1.248	–	1401				
NO_2	1.193	134.4		1346	1647		
NO_2^-	1.258	116.8		1291	1255		
NO_3	1.234	120.0				1094	1072
NO_3^-	1.260	120.0				1030	1333

System	Cu–NO (Å)	CuN–O (Å)	Cu–N–O (degree)	CuO–N (Å)	Cu–ON (Å)	Cu–O–N (degree)	Q_{Cu} a.u.	Q_{NO} a.u.	Q_{ON} a.u.	ν_{NO} (cm^{-1})	ν_{NO} (cm^{-1})
Z–^{2}CuNO	1.802	1.158	150.4				1.02	−0.16		1830	
Z–^{2}CuON				1.167	1.915	143.6	0.99		−0.10	1703	
Z–^{2}Cu–κ^2NO	1.900	1.207	73.9	1.207	1.975	70.9	1.13	−0.31		1532	
Z–^{1}Cu$(NO)_2$	1.968	1.150	126.0				1.05	−0.10	0.10	1701[c]	1857[b]
Z–^{1}Cu(NO)(ON)	1.869	1.166	110.3	1.137	2.545	122.4	1.00	−0.23	−0.14	1665[c]	1869[b]
Z–^{1}Cu$(ON)_2$				1.175	1.968	136.8	1.00			1610[c]	1748[b]

System	Cu–ON (Å)	CuO–N (Å)	ON–O (Å)	Cu–O–N (degree)	O–N–O (degree)	Q_{Cu} a.u.	Q_{NO2} a.u.	ν_{NO2} (cm^{-1})
Z–^{2}Cu–NO_2	1.805	1.354	1.179	125.0	116.2	1.29	−0.56	1605[a]
Z–^{2}Cu–κ^2NO_2	2.032	1.278	1.191	68.6	124.9	1.25	−0.47	1590[a]
Z–^{2}Cu–κ^3NO_2	2.012	1.263	1.261	94.2	110.3	1.33	−0.60	1362[c]

System	Cu–ON (Å)	CuO–N (Å)	ON–O (Å)	Cu–O–N (degree)	O–N–O (degree)	Q_{Cu} a.u.	Q_{NO3} a.u.	ν_{NO3} (cm^{-1})
Z–^{2}Cu–κ^3NO_3	2.006	1.293	1.190	91.7	124.2	1.37	−0.63	1612[a]

[a] Stretching frequency.
[b] Symmetric stretching vibration.
[c] Asymmetric stretching vibration.

structures are displayed on Figs. 3 and 4. In all cases, the angles Cu–N–O and Cu–O–N are lower than 180°, indicating that NO behaves like an anion. The anionic character of the adsorbed NO molecule can be noticed by the negative net charge values Q_{NO} and Q_{ON} (see Table 3). As expected, the Cu charge is positive and close to +1. The calculated ν_{NO} for Z–^{2}CuNO (1830 cm^{-1}) is in good agreement with the experimental values 1814 cm^{-1} [9] and 1812 cm^{-1} [42] considering the theoretical standard deviation of ±37 cm^{-1} [69]. The ν_{NO} is 86 cm^{-1} lower (red shift) than the corresponding to free NO due to the π-back donation from Cu^+ *d* electrons to NO. As the π-back donation increases, the N–O distance increases and the ν_{NO} decreases. The calculated ν_{NO} for Z–^{2}Cu–NO_2 (1605 cm^{-1}) and Z–^{2}Cu–κ^3NO_3 (1612 cm^{-1}) obtained herein are in reasonable agreement with the experimental values of 1630 cm^{-1} [44,80] and 1624 cm^{-1} [41] for $[CuNO_2]^+$ and $[CuNO_3]^+$ species, respectively.

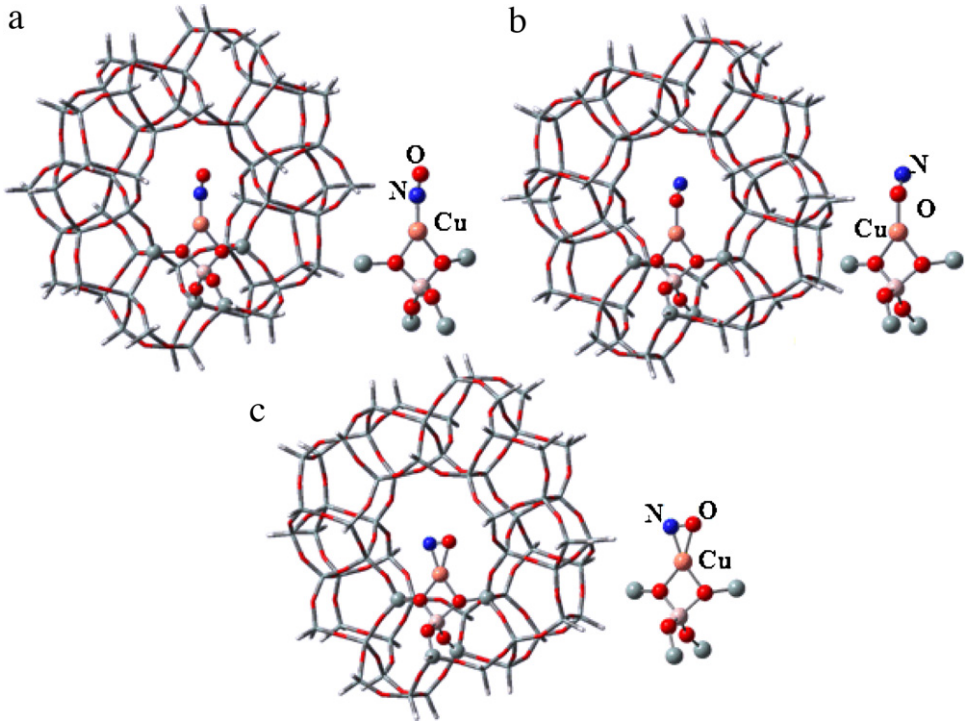

Fig. 3. Minimum energy structures: (a) κ^1–NO mode by the N atom, (b) κ^1–NO mode by the O atom and (c) κ^2–NO mode. High level, ball-stick. Low level, tube. O, red; Si, grey; Al, pink; Cu, orange and N, blue. (For interpretation of the references to color in this figure legend, the reader is referred to the web version of the article.)

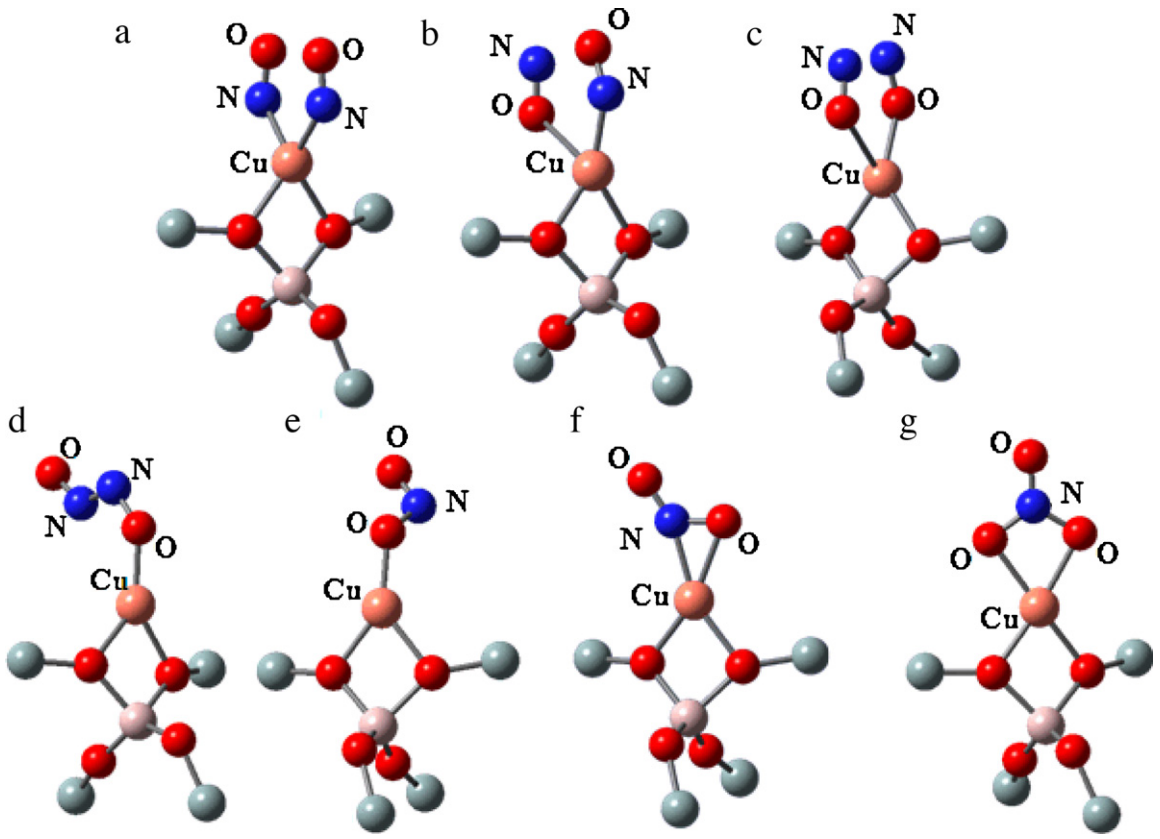

Fig. 4. Optimized structures: (a) Z–^{1}Cu(NO)$_2$, (b) Z–^{1}Cu(NO)(ON), (c) Z–^{1}Cu(ON)$_2$, (d) Z–^{1}CuONNO, (e) Z–^{2}Cu–κ^2NO$_2$, (f) Z–^{2}Cu–κ^3NO$_2$ and (g) Z–^{2}Cu–κ^3NO$_3$. O, red; Si, grey; Al, pink; Cu, orange and N, blue. The low level is not shown for better understanding. (For interpretation of the references to color in this figure legend, the reader is referred to the web version of the article.)

For the adsorption of two NO molecules, only three structures are possible: by the N atoms (Z^{1}Cu(NO)$_2$), by the O atoms (Z^{1}Cu(ON)$_2$) and a mixed form (Z–^{1}Cu(NO)(ON)). The calculated ν_{NO} values of 1857 and 1701 cm^{-1} for Z–^{1}Cu(NO)$_2$ are in good agreement with the experimental values of 1825 and 1730 cm^{-1} [9,10], and correspond to the asymmetric and symmetric stretching vibrations, respectively. For Z–^{1}Cu(ON)$_2$ and Z–^{1}Cu(NO)(ON), the calculated frequencies were 1610 cm^{-1}, 1748 cm^{-1} and 1665 cm^{-1}, 1869 cm^{-1} respectively. Despite that the higher frequency of each species are in agreement with the experimental values, the lower ones are far from then. These results suggest that the species Z–^{1}Cu(ON)$_2$ and Z–^{1}Cu(NO)(ON) could not exist or they are minorities and not observable at experimental conditions.

3.2. Thermodynamic and NO_x interaction with Cu–ZSM-5

Tables 4 and 5 show the ΔH° and ΔG° values at 850 K and 2 atm for some relevant reactions for NO_x decomposition by Z–^{1}Cu. According to the reactions (7) and (9), the adsorption of one NO by the N atom, Z–^{2}CuNO ($\Delta H^\circ = -30.8$ kcal mol^{-1}) is thermodynamically more favorable than the corresponding by the O atom, Z–^{2}CuON ($\Delta H^\circ = -14.8$ kcal mol^{-1}). These results are a consequence of the better overlapping between the N p orbitals with Cu orbitals than the overlapping between O and Cu orbitals and therefore, the interactions by the N atom are energetically more favorable than the interactions by the O atom. The calculated value of −30.8 kcal mol^{-1} is in good agreement with the values reported in the literature of −23.9 kcal mol^{-1} [42], and −29.9 kcal mol^{-1} [27]. According to our calculations, adsorption and desorption of one NO molecule by Z–^{1}Cu are barrierless processes (see Supplementary Material, Figs. A1 and A2). The Z–^{2}CuNO and Z–^{2}CuON species can adsorb a second NO by the N or O to form Z–^{1}Cu(NO)$_2$, Z–^{1}Cu(NO)(ON) and Z–^{1}Cu(ON)$_2$ (reactions (10)–(13)). While in general, the adsorption enthalpy of a second NO molecule is negative, the Gibbs free energy is positive and greater than the corresponding to the first NO molecule. Thus, under normal operating conditions, the equilibrium fraction of Z–^{1}Cu(NO)$_2$, Z–^{1}Cu(NO)(ON) and Z–^{1}Cu(ON)$_2$ will be small compared to that of Z–^{2}CuNO or Z–^{2}CuON. Due to the high adsorption energy of the first NO molecule, the Z–^{1}Cu(NO)$_2$, Z–^{1}Cu(NO)(ON) and Z–^{1}Cu(ON)$_2$ net formation reactions (reactions (15)–(17)) are exothermic, but are not very spontaneous at 850 K. At room temperature, pressure calculations (298 K and 1 atm) show that the formation of Z–^{2}CuNO (reaction (7), $\Delta G^\circ = -18.1$ kcal mol^{-1}), Z–^{2}CuON (reaction (9), $\Delta G^\circ = -3.1$ kcal mol^{-1}), and Z–^{1}Cu(NO)$_2$ (reaction (15), $\Delta G^\circ = -5.6$ kcal mol^{-1}) species are spontaneous and therefore all these species could be present at the reaction site simultaneously. Clearly, at high temperatures the equilibrium fraction of species such as Z–^{1}Cu(NO)$_2$, Z–^{1}Cu(ON)$_2$ or Z–^{1}Cu(NO)(ON) will be low compared to that of Z–^{2}CuNO or Z–^{2}CuON. This result is consistent with experimental IR studies which show that Z–^{2}CuNO and Z–^{1}Cu(NO)$_2$ species coexist in equilibrium at room temperature [9,42,43] but not at 773 K [39]. Increasing the temperature, the Z–^{1}Cu(NO)$_2$ concentration decreases faster than the Z–^{2}CuNO or Z–^{2}CuON concentration.

Additionally to the Z–^{2}CuNO and Z–^{2}CuON species, another local minimum was found where the NO is bonded to the Cu atom by the N and O atoms (Z–^{2}Cu–κ^2NO). Starting from Z–^{1}Cu and NO, the Z–^{2}Cu–κ^2NO formation is exothermic (reaction (8)). As far as we know, this is the first time that a κ^2NO adsorption is reported. The NO interaction with the metallic center produces an enlargement of the N–O distance from 1.15 to 1.21 Å and a strong red

Table 4
ΔH° and ΔG° (kcal mol^{-1}) values at 850.15 K and 2 atm for NO adsorption and N_2O, N_2 formation.

Reaction		ΔH°	ΔG°
NO adsorption			
$Z{-}^1Cu_{(s)} + NO_{(g)} \leftrightharpoons Z{-}^2CuNO_{(s)}$	(7)	−30.8	−6.9
$Z{-}^1Cu_{(s)} + NO_{(g)} \leftrightharpoons Z{-}^2Cu{-}\kappa^2NO_{(s)}$	(8)	−19.2	6.6
$Z{-}^1Cu_{(s)} + NO_{(g)} \leftrightharpoons Z{-}^2CuON_{(s)}$	(9)	−14.8	6.9
$Z{-}^2CuNO_{(s)} + NO_{(g)} \leftrightharpoons Z{-}^1Cu(NO)_{2(s)}$	(10)	−0.7	28.1
$Z{-}^2CuNO_{(s)} + NO_{(g)} \leftrightharpoons Z{-}^1Cu(NO)(ON)_{(s)}$	(11)	6.3	36.3
$Z{-}^2CuON_{(s)} + NO_{(g)} \leftrightharpoons Z{-}^1Cu(NO)(ON)_{(s)}$	(12)	−9.7	22.5
$Z{-}^2CuON_{(s)} + NO_{(g)} \leftrightharpoons Z{-}^1Cu(ON)_{2(s)}$	(13)	−3.5	26.2
$Z{-}^2CuON_{(s)} + NO_{(g)} \leftrightharpoons\leftrightharpoons Z{-}^3CuONNO_{(s)}$	(14)	−0.3	31.5
Net reactions for two NO adsorption			
$Z{-}^1Cu_{(s)} + 2NO_{(g)} \leftrightharpoons Z{-}^1Cu(NO)_{2(s)}$	(15)	−31.5	21.2
$Z{-}^1Cu_{(s)} + 2NO_{(g)} \leftrightharpoons Z{-}^1Cu(NO)(ON)_{(s)}$	(16)	−24.5	29.4
$Z{-}^1Cu_{(s)} + 2NO_{(g)} \leftrightharpoons Z{-}^1Cu(ON)_{2(s)}$	(17)	−18.4	33.1
Interconvertion net reactions			
$Z{-}^2CuNO_{(s)} \leftrightharpoons Z{-}^2Cu{-}\kappa^2NO_{(s)}$	(18)	11.0	11.7
$Z{-}^2Cu{-}\kappa^2NO_{(s)} \leftrightharpoons Z{-}^2CuON_{(s)}$	(19)	4.6	3.3
N_2O formation			
$Z{-}^2CuNO_{(s)} + NO_{(g)} \leftrightharpoons Z{-}^1CuO_{(s)} + N_2O_{(g)}$	(20)	33.8	47.4
$Z{-}^2CuNO_{(s)} + NO_{(g)} \leftrightharpoons Z{-}^3CuO_{(s)} + N_2O_{(g)}$	(21)	9.0	19.6
$Z{-}^2CuON_{(s)} + NO_{(g)} \leftrightharpoons Z{-}^1CuO_{(s)} + N_2O_{(g)}$	(22)	17.8	33.6
$Z{-}^2CuON_{(s)} + NO_{(g)} \leftrightharpoons Z{-}^3CuO_{(s)} + N_2O_{(g)}$	(23)	−6.9	5.8
$Z{-}^1Cu(NO)_{2(s)} \leftrightharpoons Z{-}^1CuO_{(s)} + N_2O_{(g)}$	(24)	34.5	19.2
$Z{-}^1Cu(NO)(ON)_{(s)} \leftrightharpoons Z{-}^1CuO_{(s)} + N_2O_{(g)}$	(25)	27.5	11.1
$Z{-}^1Cu(ON)_{2(s)} \leftrightharpoons Z{-}^1CuO_{(s)} + N_2O_{(g)}$	(26)	21.4	7.4
$Z{-}^3CuONNO_{(s)} \leftrightharpoons Z{-}^3CuO_{(s)} + N_2O_{(g)}$	(27)	−6.6	−25.7
Net reactions for N_2O formation from two NO adsorption			
$Z{-}^1Cu_{(s)} + 2NO_{(g)} \leftrightharpoons Z{-}^1CuO_{(s)} + N_2O_{(g)}$	(28)	3.0	40.5
$Z{-}^1Cu_{(s)} + 2NO_{(g)} \leftrightharpoons Z{-}^3CuO_{(s)} + N_2O_{(g)}$	(29)	−21.7	12.8
$Z{-}^1CuO_{(s)} \leftrightharpoons Z{-}^3CuO_{(s)}$	(30)	−24.7	−27.7
N_2 formation			
$Z{-}^1CuO_{(s)} + N_2O_{(g)} \leftrightharpoons Z{-}^1Cu{-}\kappa^1O_{2(s)} + N_{2(g)}$	(31)	−23.8	−34.1
$Z{-}^3CuO_{(s)} + N_2O_{(g)} \leftrightharpoons Z{-}^3Cu{-}\kappa^1O_{2(s)} + N_{2(g)}$	(32)	−14.2	−31.8
$Z{-}^1CuO_{(s)} + N_2O_{(g)} \leftrightharpoons Z{-}^1Cu{-}\kappa^2O_{2(s)} + N_{2(g)}$	(33)	−34.5	−40.1
$Z{-}^3CuO_{(s)} + N_2O_{(g)} \leftrightharpoons Z{-}^3Cu{-}\kappa^2O_{2(s)} + N_{2(g)}$	(34)	−23.7	−32.6
$Z{-}^1Cu_{(s)} + N_2O_{(g)} \leftrightharpoons Z{-}^1CuON_{2(s)}$	(35)	−19.8	11.0
$Z{-}^1CuON_{2(s)} \leftrightharpoons Z{-}^1CuO_{(s)} + N_{2(g)}$	(36)	45.4	5.8
$Z{-}^1CuON_{2(s)} \leftrightharpoons Z{-}^3CuO_{(s)} + N_{2(g)}$	(37)	20.6	−21.9
$Z{-}^1Cu_{(s)} + N_2O_{(g)} \leftrightharpoons Z{-}^1CuO_{(s)} + N_{2(g)}$	(38)	25.6	16.8
$Z{-}^1Cu_{(s)} + N_2O_{(g)} \leftrightharpoons Z{-}^3CuO_{(s)} + N_{2(g)}$	(39)	0.8	−10.9

Table 5
ΔH° and ΔG° (kcal mol^{-1}) values at 850.15 K and 2 atm for NO_2, NO_3 formation and O_2 desorption.

Reaction		ΔH°	ΔG°
NO_2 formation			
$Z{-}^1CuO_{(s)} + NO_{(g)} \leftrightharpoons Z{-}^2Cu{-}NO_{2(s)}$	(40)	−66.1	−41.5
$Z{-}^3CuO_{(s)} + NO_{(g)} \leftrightharpoons Z{-}^2Cu{-}NO_{2(s)}$	(41)	−41.4	−13.8
$Z{-}^1CuO_{(s)} + NO_{(g)} \leftrightharpoons Z{-}^2Cu{-}\kappa^2NO_{2(s)}$	(42)	−72.7	−44.2
$Z{-}^3CuO_{(s)} + NO_{(g)} \leftrightharpoons Z{-}^2Cu{-}\kappa^2NO_{2(s)}$	(43)	−47.9	−16.5
$Z{-}^1CuO_{(s)} + NO_{(g)} \leftrightharpoons Z{-}^2Cu{-}\kappa^3NO_{2(s)}$	(44)	−77.5	−47.8
$Z{-}^3CuO_{(s)} + NO_{(g)} \leftrightharpoons Z{-}^2Cu{-}\kappa^3NO_{2(s)}$	(45)	−52.7	−20.0
NO_2 desorption			
$Z{-}^2Cu{-}NO_{2(s)} \leftrightharpoons Z{-}^1Cu_{(s)} + NO_2$	(46)	18.5	34.1
$Z{-}^2Cu{-}\kappa^2NO_{2(s)} \leftrightharpoons Z{-}^1Cu_{(s)} + NO_2$	(47)	25.1	36.7
$Z{-}^2Cu{-}\kappa^3NO_{2(s)} \leftrightharpoons Z{-}^1Cu_{(s)} + NO_2$	(48)	29.8	40.3
NO_3 formation			
$Z{-}^1CuO_{(s)} + NO_{2(g)} \leftrightharpoons Z{-}^2Cu{-}\kappa^3NO_{3(s)}$	(49)	−76.9	−81.7
$Z{-}^3CuO_{(s)} + NO_{2(g)} \leftrightharpoons Z{-}^2Cu{-}\kappa^3NO_{3(s)}$	(50)	−52.2	−54.0
NO_3 decomposition			
$Z{-}^2Cu{-}\kappa^3NO_{3(s)} \leftrightharpoons Z{-}^1Cu{-}\kappa^1O_{2(s)} + NO_{(g)}$	(51)	75.2	38.4
$Z{-}^2Cu{-}\kappa^3NO_{3(s)} \leftrightharpoons Z{-}^3Cu{-}\kappa^1O_{2(s)} + NO_{(g)}$	(52)	59.9	12.8
$Z{-}^2Cu{-}\kappa^3NO_{3(s)} \leftrightharpoons Z{-}^1Cu{-}\kappa^2O_{2(s)} + NO_{(g)}$	(53)	64.4	32.3
$Z{-}^2Cu{-}\kappa^3NO_{3(s)} \leftrightharpoons Z{-}^3Cu{-}\kappa^2O_{2(s)} + NO_{(g)}$	(54)	50.4	12.1
O_2 desorption			
$Z{-}^1Cu{-}\kappa^1O_{2(s)} \leftrightharpoons Z{-}^1Cu_{(s)} + {}^1O_{2(g)}$	(55)	33.1	9.9
$Z{-}^3Cu{-}\kappa^1O_{2(s)} \leftrightharpoons Z{-}^1Cu_{(s)} + {}^3O_{2(g)}$	(56)	9.8	−4.86
$Z{-}^1Cu{-}\kappa^2O_{2(s)} \leftrightharpoons Z{-}^1Cu_{(s)} + {}^1O_{2(g)}$	(57)	43.9	16.4
$(58) Z{-}^3Cu{-}\kappa^2O_{2(s)} \leftrightharpoons Z{-}^1Cu_{(s)} + {}^3O_{2(g)}$		19.3	−4.1
O_2 displacement by NO			
$(59) Z{-}^1Cu{-}\kappa^1O_{2(s)} + NO_{(g)} \leftrightharpoons Z{-}^2CuNO_{(s)} + {}^1O_{2(g)}$		2.4	3.1
$(60) Z{-}^1Cu{-}\kappa^2O_{2(s)} + NO_{(g)} \leftrightharpoons Z{-}^2CuNO_{(s)} + {}^1O_{2(g)}$		13.1	9.2
$(61) Z{-}^3Cu{-}\kappa^1O_{2(s)} + NO_{(g)} \leftrightharpoons Z{-}^2CuNO_{(s)} + {}^3O_{2(g)}$		−20.9	−11.7
$(62) Z{-}^3Cu{-}\kappa^2O_{2(s)} + NO_{(g)} \leftrightharpoons Z{-}^2CuNO_{(s)} + {}^3O_{2(g)}$		−11.5	−11.0

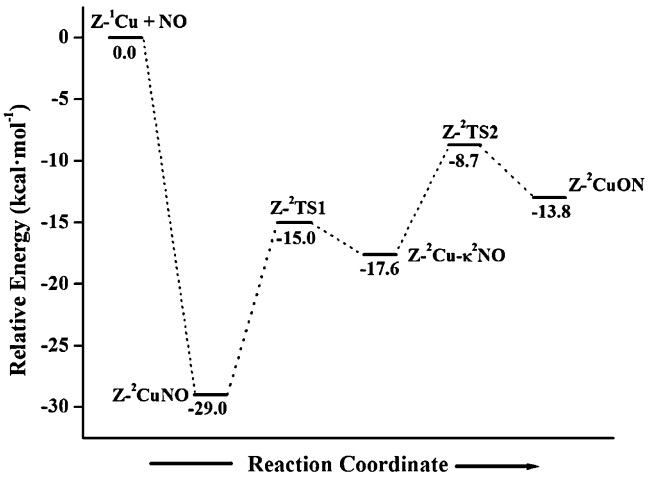

Fig. 5. Potential energy surface (PES) of $Z{-}^2CuNO$, $Z{-}^2CuON$ and $Z{-}^2Cu{-}\kappa^2NO$ species interconversion. The relative energies are with respect to $Z{-}^1Cu$ + NO species.

shift of 384 cm^{-1} (1532 cm^{-1}) which indicates considerable charge transferred from the Cu to NO molecule. In order to explore if the $Z{-}^2CuNO$, $Z{-}^2Cu{-}\kappa^2NO$ and $Z{-}^2CuON$ species are interconnected by a reaction pathway, a potential energy surface calculation was performed (see Fig. 5). The results indicate that in a first step, the $Z{-}^2CuNO$ (at the left of Fig. 5) could be converted to $Z{-}^2Cu{-}\kappa^2NO$ passing through the $Z{-}^2TS1$ transition structure with an activation energy of 14 kcal mol^{-1} (imaginary frequency of −358 cm^{-1}). Analogously, the $Z{-}^2Cu{-}\kappa^2NO$ could be converted to $Z{-}^2CuON$ passing through the $Z{-}^2TS2$ transition structure with a less activation energy of 8.9 kcal mol^{-1} (imaginary frequency of −323 cm^{-1}) (see Fig. 5). These moderate values obtained for the activation energies indicate that the $Z{-}^2CuNO$, $Z{-}^2CuON$ and $Z{-}^2Cu{-}\kappa^2NO$ species could be present simultaneously at the reaction site in a dynamic equilibrium.

There is some evidence in the literature that N_2O is formed during the reduction of NO [38,41,44–46,72]. To shed some light on this problem, we have undertaken quantum chemical modeling of the N_2O formation (reactions (20)–(30)). The NO adsorbed (NO_{ads}) on $Z{-}^1Cu$ ($Z{-}^2CuNO$ or $Z{-}^2CuON$) can react with one NO molecule to produce N_2O plus Z–CuO. Some authors [44–46] have proposed that this reaction can occur in two steps; first, the formation of some kind of $Z{-}^1Cu(NO)_2$ species followed by the decomposition of this species in N_2O and one adsorbed O atom (O_{ads}). According to the results presented in Table 4, the most favorable reactions for N_2O formation are the reactions (23) and (27), and the less favorable are 20 and 22. This is a consequence of the fact that the $Z{-}^3CuO$ species is energetically more stable than $Z{-}^1CuO$ species. Consequently, reactions with $Z{-}^1CuO$ species formation are thermodynamically less favorable than those with $Z{-}^3CuO$ species formation. Schneider and coworkers [44,45] proposed that the N_2O is produced by the interaction of $Z{-}^2CuON$ species with NO, while Bell and coworkers [39,40] proposed that the interaction of $Z{-}^2CuNO$ with NO to produce N_2O. They reported that both paths are thermodynamically favorable and therefore possible reactions of the mechanism. Our results show that both species $Z{-}^2CuON$ and $Z{-}^2CuNO$ are interconnected through the $Z{-}^2Cu{-}\kappa^2NO$ species with moderate values of activation energies. Therefore, there are two possibilities for N_2O formation: first, the $Z{-}^2CuON$ as well as $Z{-}^2CuNO$ species coexist at the experimental reaction conditions, interconnected by $Z{-}^2Cu{-}\kappa^2NO$ and the N_2O is produced by both species. Second, at the first step the NO is adsorbed only by the N atom producing the $Z{-}^2CuNO$ species, which changes to $Z{-}^2CuON$ through $Z{-}^2Cu{-}\kappa^2NO$ intermediate. The NO interacts with $Z{-}^2CuON$ to produce the corresponding products.

According to Schneider and coworkers [45], NO reacts with Z–^{2}CuON to produce the Z–^{3}CuONNO species, which decomposes to N_2O and Z–CuO with an activation barrier of 7 kcal mol^{-1}. Although, this reaction has a low activation barrier, at 850 K it is only slightly exothermic (reaction (14)) and the positive ΔG value indicates that this is in an unfavorable process. Unfortunately, the reaction pathway with the Z–^{2}CuNO species has not been reported yet. Therefore, it is not possible to conclude which pathway is the most feasible. The aforementioned results seem to indicate that there is a compromise between kinetic and thermodynamic in the N_2O formation. High temperatures favor the kinetic but disfavor the thermodynamic of the reaction.

According to the proposed mechanisms in the literature, the N_2 formation can occur from N_2O and Z–^{3,1}CuO [39,40,44,45] (reactions (31)–(34)) or from N_2O decomposition by the active site [46] reactions (35)–(37). In general, N_2O decomposition by Z–^{3,1}CuO is thermodynamically more favored than the corresponding by the active site. The calculations show that the overall reaction of Z–^{1}Cu with one N_2O molecule to produce Z–^{3}CuO plus one N_2 molecule (reaction (39)) (ΔH° = +0.8 kcal mol^{-1} and ΔG° = −10.9 kcal mol^{-1}) is thermodynamically more favored than the corresponding to the singlet state product formation Z–^{1}CuO (reaction (38)) (ΔH° = +25.6 kcal mol^{-1} and ΔG° = +16.8 kcal mol^{-1}). This is a consequence of the greater stability of Z–^{3}CuO with respect to the Z–^{1}CuO species. According to the former discussion, the N_2O decomposition is thermodynamically feasible by two paths: reaction (35) followed by (37) or the reduction by the Z–^{3}CuO or Z–^{1}CuO species (reactions (31)–(34)). As we have not determined activation barriers, it is not possible to conclude which pathway is the most probable.

In the mechanisms proposed in the literature [39,40,44–46] the active site, Z–^{1}Cu, is regenerated by O_2 desorption (reactions (55)–(58)). Herein, the calculated ΔH° value for O_2 adsorption (reverse reaction (58)) −19.3 kcal mol^{-1} is in good agreement with the experimental value of −18 kcal mol^{-1} [46] pointing out that if Z–Cu is the active site, the O_2 will be adsorbed in a κ^2 mode. As expected, the O_2 desorption (reactions (56) and (58)) is thermodynamically favored at 850 K. However, the O_2 displacement by NO (reactions (61) and (62)) are more favored thermodynamically than the corresponding to O_2 desorption therefore it is likely that in the reaction condition the active site is regenerated by reaction (61) or (62) instead of O_2 desorption.

Iglesia and coworkers [46] have proposed a series of reactions among NO, O_2 and NO_2 to guarantee the quasi-equilibrium nature for the O_2 desorption. NO interacts with O_{ads} on Z–^{1}Cu (reactions (40)–(45), Table 5) to form NO_2, which in a second step is liberated (reactions (46)–(48)). After that, NO_3 is formed (reactions (49) and (50)) followed by its decomposition (reactions (51)–(54)) and, in a final step, O_2 is desorbed (reactions (55)–(58)). Table 5 shows that NO_2 formation from Z–^{1,3}CuO plus NO is thermodynamically favored but its desorption is not (reactions (46)–(48)) in agreement with previously published results [39]. On the other hand, the NO_3 formation (reactions (49) and (50)) is thermodynamically very favorable but its decomposition into Z–CuO_2 plus NO is not. According to the above discussion, it seems likely that the NO_2 and NO_3 formation from a thermodynamic standpoint is the driving force of the O_2 formation in the mechanism proposed by Iglesia and coworkers [46].

4. Conclusions

Using DFT–ONIOM calculations we have examined the structural, geometric, vibrational and thermodynamic properties of some possible intermediates involved in the DCD-NO_x catalyzed by the Cu–ZSM-5. The most relevant aspects of this work are:

(a) Calculations of vibrational frequencies for the interaction of the Z–Cu system with N_2, H_2, NO, NO_2 and NO_3 molecules as well as the N_2, NO and O_2 adsorption heats, show good agreement with experimental data. This suggests that a representative model and adequate methodology have been selected.
(b) For the first time the Z–^{2}Cu–κ^2NO species which is in a dynamic equilibrium with the Z–^{2}CuNO and Z–^{2}CuON species is reported. The low activation barriers (13.9 and 8.8 kcal mol^{-1}) for the pathways connecting the Z–^{2}CuNO, Z–^{2}CuON and Z–^{2}Cu–κ^2NO point out that both Z–^{2}Cu–NO and Z–^{2}Cu–ON species could be present at the reaction conditions.
(c) The analysis of the ΔH° and ΔG° shows, from a thermodynamic standpoint, that active site is regenerated by the reaction of O_2 displacement by NO and in lesser extent by the O_2 desorption.
(d) Desorption of NO_2 and NO_3 decomposition reactions is not thermodynamically favored, if these processes occur in the reaction medium it is because the reactions are kinetically controlled.

Acknowledgements

The authors gratefully acknowledge the financial support from the National Science and Technology Fund (FONACIT – Grant No. G-2005000426).

Appendix A. Supplementary data

Supplementary data associated with this article can be found, in the online version, at doi:10.1016/j.molcata.2011.07.018.

References

[1] B.J. Finlayson-Pitts, J.N. Pitts Jr., Science 276 (1997) 1045–1052.
[2] J.N. Galloway, A.R. Townsend, J.W. Erisman, M. Benkunda, Z. Cai, J.R. Freney, L.A. Martinelli, S.P. Seitzinger, M.A. Sutton, Science 320 (2008) 889–892.
[3] C.J. Howard, W. Yang, P.G. Green, F. Mitlochner, I.L. Malkina, R.G. Flocchini, M.J. Kleeman, Atmospheric Environment 42 (2008) 5267–5277.
[4] K. Butterbach-Bahl, M. Kahl, L. Mykhayliv, C. Werner, R. Kiese, A.C. Li, Atmos. Environ. 43 (2008) 1392–1402.
[5] R.A. Duce, J. LaRoche, K. Altierri, K.R. Arrigo, A.R. Baker, D.G. Capone, S. Cornell, F. Dentener, J. Galloway, R.S. Ganeshram, R.J. Geider, T. Jickells, M.M. Kuypers, R. Langlois, P.S. Liss, S.M. Liu, J.J. Middelburrg, C.M. Moore, S. Nickovic, A. Oschlies, T. Pedersen, J. Prospero, S. Schlitzer, L.L. Sorensen, M. Uematsu, O. Ulloa, M. Voss, B. Ward, L. Zamora, Science 320 (2008) 893–897.
[6] N.V. Heeb, C.J. Saxer, A.M. Forss, S. Brühlmann, Atmos. Environ. 42 (2008) 2543–2554.
[7] C.Y. Sung, L.J. Broadbelt, R.Q. Snurr, Catal. Today 136 (2008) 64–75.
[8] C-J. Shiu, S.C. Liu, C-C. Chang, J-P. Chen, C.C.J. Chou, C-Y. Lin, C-Y. Young, Atmos. Environ. 41 (2007) 9324–9340.
[9] P. Pietrzyk, B. Gil, Z. Sojka, Catal. Today 126 (2007) 103–111.
[10] P. Pietrzyk, F. Zasada, W. Piskorz, A. Kotarba, Z. Sojka, Catal. Today 119 (2007) 219–227.
[11] R. Ramprasad, K.C. Hass, W.F. Schneider, J.B. Adams, J. Phys. Chem. B 101 (1997) 6903–6913.
[12] F. Schüth, Angew. Chem. Int. Ed. 42 (2003) 3604–3622.
[13] B. Jansang, T. Nanok, J. Limtrakul, J. Phys. Chem. C 112 (2008) 540–547.
[14] A. Goursot, B. Coq, F. Fajula, J. Catal. 216 (2003) 324–332.
[15] M. García-Sánchez, P.C.M.M. Magusin, E.J.M. Hensen, P.C. Thüne, X. Rozanska, R.A. Van Santen, J. Catal. 219 (2003) 352–361.
[16] A.V. Larin, G.M. Zhidomirov, D.N. Trubnicov, D.P. Vercauteren, J. Mol. Catal. A 305 (2009) 90–94.
[17] K. Sillar, P. Burk, J. Phys. Chem. B 108 (2004) 9893–9899.
[18] F. Ruette, M. Sánchez, A. Sierraalta, C. Mendoza, R. Añez, L. Rodríguez, O. Lisboa, J. Daza, P. Manrique, Z. Perdomo, M. Rosa-Brussin, J. Mol. Catal. A 228 (2005) 211–225.
[19] Z. Schay, L. Guczi, A. Beck, I. Nagy, V. Samuel, Mirajkar, A.B. Ramaswamy, G. Pál-Borbély, Catal. Today 75 (2002) 393–399.
[20] Q. Sun, W.M.H. Sachtler, Appl. Catal. B 42 (2003) 393–401.
[21] D. Berthomieu, N. Jardillier, G. Delahay, B. Coq, A. Goursot, Catal. Today 110 (2005) 294–302.
[22] J.N. Armor, Catal. Today 26 (1995) 147–158.
[23] J.A.Z. Piterse, S. Booneveld, Appl. Catal. B 73 (2007) 327–335.
[24] G. Qi, R.T. Yang, L.T. Thompson, Appl. Catal. A 259 (2004) 261–267.
[25] Y-W. Lee, E. Gulari, Catal. Commun. 5 (2004) 499–503.
[26] N. Macleod, R. Cropley, J.M. Keel, R.M. Lambert, J. Catal. 221 (2004) 20–31.
[27] M. Davidová, D. Nachtigallová, P. Nachtigall, J. Sauer, J. Phys. Chem. B 108 (2004) 13674–13682.

[28] M. Iwamoto, S. Yokoo, K. Sacay, S. Kagawa, J. Chem. Soc. Faraday Trans. 1 (1980) 1629–1638.
[29] M. Iwamoto, H. Furukawa, Y. Mine, F. Uemura, S. Micuriya, S. Kagawa, J. Chem. Soc. Chem. Commun. 111 (1986) 1272–1273.
[30] Y. Li, K.W. Hall, J. Catal. 129 (1991) 202–215.
[31] L. Lisi, R. Pirone, G. Ruoppolo, G. Russo, Kinet. Catal. 49 (2008) 421–427.
[32] F. Poignant, J.L. Freysz, M. Daturi, J. Saussey, Catal. Today 70 (2001) 197–211.
[33] L. Guangfeng, W. Xinping, J. Cuiying, L. Zhiguang, J. Catal. 257 (2008) 291–296.
[34] F. Garin, Appl. Catal. A 222 (2001) 183–219.
[35] V.B. Kazanky, E.A. Pidko, Catal. Today 110 (2005) 281–293.
[36] J. Dědeček, L. Čapek, B. Wichterlová, Appl. Catal. A 307 (2006) 156–164.
[37] B. Coq, G. Delahay, R. Durand, D. Berthomieu, E. Ayala-Villagomez, J. Phys. Chem. B 108 (2004) 11062–11068.
[38] H. Yahiro, M. Iwamoto, Appl. Catal. A 222 (2001) 163–181.
[39] B.L. Trout, A.K. Chakraborty, A.T. Bell, J. Phys. Chem. 100 (1996) 17582–17592.
[40] A.T. Bell, Catal. Today 38 (1997) 151–156.
[41] M.V. Konduru, S.S.C. Chuang, X. Kang, J. Phys. Chem. B 105 (2001) 10918–10926.
[42] J. Datka, P. Kozyra, E. Kukulska-Zajac, Catal. Today 90 (2004) 109–114.
[43] G. Spoto, A. Zecchina, S. Bordiga, G. Ricchiardi, G. Martra, G. Leofanti, G. Petrini, Appl. Catal. B 3 (1994) 151–172.
[44] W.F. Schneider, K.C. Hass, R. Ramprasad, J.B. Adams, J. Phys. Chem. B 102 (1998) 3692–3705.
[45] W.F. Schneider, K.C. Hass, R. Ramprasad, J.B. Adams, J. Phys. Chem. B 101 (1997) 4353–4357.
[46] B. Moden, P. Da Costa, B. Fonfe, D.K. Lee, E. Iglesia, J. Catal. 209 (2002) 75–86.
[47] I.I. Zakharov, Z.R. Ismagilov, S.Ph. Ruzankin, V.F. Anufrienko, S.A. Yashnik, O.I. Zakharova, J. Phys. Chem. C 111 (2007) 3080–3089.
[48] X. Solans-Monfort, V. Branchadell, M. Sodupe, J. Phys. Chem. B 106 (2002) 1372–1379.
[49] D. Segupta, J.B. Adams, W.F. Schneider, K.C. Hass, Catal. Lett. 74 (2001) 193–199.
[50] A. Sierraalta, A. Bermudez, M. Rosa-Brussin, J. Mol. Catal. A 228 (2005) 203–228.
[51] A. Sierraalta, R. Añez, M. Rosa-Brussin, J. Catal. 205 (2002) 107–114.
[52] A. Pulido, P. Nachtigall, Phys. Chem. Chem. Phys. 11 (2009) 1447–1458.
[53] K. Koszinowski, D. Shröder, M. Shwarz, M.C. Holthausen, J. Sauer, H. Koizumi, P.B. Armentrout, Inorg. Chem. 41 (2002) 5882–5890.
[54] Y. Zhang, Y. Sun, A. Cao, J. Liu, G. Fan, J. Mol. Struct. (THEOCHEM) 623 (2003) 245–251.
[55] A. Delabie, K. Pierloot, J. Phys. Chem. A 106 (2002) 5679–5685.
[56] C. Bo, F. Maseras, Dalton Trans. (2008) 2911–2919.
[57] I.H. Hillier, J. Mol. Struct. (THEOCHEM) 463 (1999) 45–52.
[58] M. Elstner, T. Frauenheim, S. Suhai, J. Mol. Struct. (THEOCHEM) 632 (2003) 29–41.
[59] S. Dapprich, I. Komáromi, K. Suzie-Byun, K. Morokuma, M.J. Frisch, J. Mol. Struct. (THEOCHEM) 461–462 (1999) 1–21.
[60] T. Kerdcharoen, K. Morokuma, Chem. Phys. Lett. 355 (2002) 257–262.
[61] K. Morokuma, Bull. Kor. Chem. Soc. 24 (6) (2003) 797–801.
[62] W.A.M. Joshi, N. Delgass, K.T. Thomson, J. Phys. Chem. C 111 (2007) 11888–11896.
[63] F. Bonino, A. Damin, G. Ricchiardi, M. Ricci, G. Spanò, R. D'Aloisio, A. Zecchina, C. Lamberti, C. Prestipino, S. Bordiga, J. Phys. Chem. B 108 (2004) 3573–3583.
[64] P. Mignon, P. Geerlings, R. Schoonheydt, J. Phys. Chem. B 110 (2006) 24947–24954.
[65] W.A.M. Joschi, N. Delgass, K.D. Thomson, J. Phys. Chem. C 111 (2007) 7841–7844.
[66] M.J. Frisch, et al., GAUSSIAN03, Gaussian Inc., Pittsburgh, PA, 2003.
[67] A.K. Rappé, C.J. Casewit, K.S. Colwell, W.A. Goddard, W.M. Skiff, J. Am. Chem. Soc. 114 (1992) 10024.
[68] www. gaussian.com/g_ur/m_basis_sets.htm.
[69] M.P. Andersson, P. Uvdal, J. Phys. Chem. A 109 (2005) 2937–2941.
[70] K.B. Wiberg, Tetrahedron 24 (1968) 1083–1096.
[71] A.E. Reed, L.A. Curtiss, F. Weinhold, Chem. Rev. 88 (1988) 899–926.
[72] M. Iwamoto, H. Yahiro, Y. Mine, S. Kagawa, Chem. Lett. 21 (1989) 3–216.
[73] C. Lamberti, S. Bordiga, M. Salvalaggio, G. Spoto, A. Zecchina, F. Geobaldo, G. Vlaic, M. Bellatreccia, J. Phys. Chem. B 101 (1997) 344–360.
[74] D. Nachtigallová, P. Nachtigall, M. Sierka, J. Sauer, Phys. Chem. Chem. Phys. 1 (1999) 2019–2026.
[75] P. Spuhler, M.C. Holthausen, D. Nachtigallova, P. Nachtigall, J. Sauer, Chem. Eur. J. 8 (2002) 2099–2115.
[76] G.T. Palomino, P. Fisicaro, S. Bordiga, A. Zecchina, E. Giamello, C. Lamberti, J. Phys. Chem. B 104 (2000) 4064–4073.
[77] J. Dedecek, L. Capek, B. Wichterlová, Appl. Catal. A: General 307 (2006) 156–164.
[78] Y. Kuroda, Y. Yosshikawa, S. Emura, R. Kumashiro, M. Nagao, J. Phys. Chem. B 103 (1999) 2155–2164.
[79] V.P. Kasansky, E.A. Pidko, Catal. Today 110 (2005) 281–293.
[80] Y. Kuroda, R. Kumashiro, T. Yoshimoto, M. Nagao, Phys. Chem. Chem. Phys. 1 (1999) 649–656.